Metallic particle manipulation with adjustable trapping range through customized field

Bai, Zhidong; Zhang, Shuoshuo; Lyu, Yudong; Zhao, Rui; Yue, Xifu; Ge, Xiaolu; Fu, Shenggui; Man, Zhongsheng

DOI
10.1016/j.optcom.2020.126045

Publication date
2020

Document Version
Final published version

Published in
Optics Communications

Optics Communications 473 (2020) 126045

Contents lists available at ScienceDirect

Optics Communications

journal homepage: www.elsevier.com/locate/optcom

Metallic particle manipulation with adjustable trapping range through customized field

Zhidong Bai [a], Shuoshuo Zhang [a], Yudong Lyu [a], Rui Zhao [a], Xifu Yue [a], Xiaolu Ge [a], Shenggui Fu [a], Zhongsheng Man [a,b,c,*]

[a] School of Physics and Optoelectronic Engineering, Shandong University of Technology, Zibo 255000, China
[b] Optics Research Group, Delft University of Technology, Department of Imaging Physics, Lorentzweg 1, 2628CJ Delft, The Netherlands
[c] Collaborative Innovation Center of Light Manipulations and Applications, Shandong Normal University, Jinan 250358, China

ARTICLE INFO

Keywords:
Optical tweezers
Nanoparticles
Optical trapping
Trapping range

ABSTRACT

Since the invention of optical tweezers, optical manipulation has advanced significantly in many applications, including atomic physics, biochemistry and soft matter physics. Here, we propose a method to trap metallic particles with adjustable trapping range in the transverse plane with the help of customized field. By tailoring the polarization state of the incident field, the focal field with elongation in the direction perpendicular to optical axis can be turned in the 4π focusing system. As a result, optical trapping with tunable trapping range is possible when the metallic particle is interacted with such customized field.

1. Introduction

Maxwell's classical electromagnetic field theory shows that the momentum transfer from an electromagnetic field to an object will produce optical pressure on that object. However, because this force is rather small, laboratory demonstrations of the phenomenon were extremely difficult. The acceleration and trapping of micron-sized particles using optical pressure was first demonstrated experimentally by Ashkin et al. in 1970 [1]. This work established the foundation for the subsequent realization of laser trapping [2] and atomic cooling [3]. It was not until 1986 that Ashkin developed a three-dimensional (3D) stable optical trap based on a single-beam gradient force [3], which is now commonly known as optical tweezers. Since then, optical tweezers have been used successfully in a wide-ranging series of studies, from the trapping and modification of nanometer-scale materials [4–8] to measurement of force with femtonewton resolution [9,10]. In recent years, various optical fields have been used for observation research, layout assembly and modification processing of particles to meet the needs of different applications [11–14]. To date, stable optical trapping and manipulation of subnanometer- to micrometer-scale particles has been demonstrated extensively using optical traps composed of a continuous-wave Gaussian laser beam [15,16], a cylindrical vector beam [17,18], an evanescent field [19], a highly focused plasmonic field [20] and spinning light fields [21,22].

In optical tweezers applications, the ability to manipulate particles over relatively long distances is essential in determining overall process efficiency. In order to maximize manipulation range, it is necessary to increase the optical trap range, which, however, is often accompanied by the destruction of stable trapping conditions due to decrease of optical intensity gradient. As such, numerous efforts have been devoted to the development of original optical tweezers configurations in conjunction with optimized illumination conditions that can simultaneously enlarge the trapping range and enable 3D manipulation of multiple metallic nanoparticles [23–32]. Although stable 3D trapping with multiple equilibrium locations can be achieved within a large focal region by appropriate adjustment of the focusing conditions, this type of trapping can only be achieved along the optical axis and, to the best of our knowledge, there have been few reports concerning trapping in the transverse direction. Recently, a method for particle trapping and manipulation using a mirror-symmetric optical vortex beam has been reported [33]. However, only two-dimensional trapping of yeast cells has been verified thus far, although the transverse trapping range of this technique is three times longer than that of the Gaussian beam-based technique. Therefore, enlargement of the transverse trapping range while simultaneously ensuring stable 3D trapping of metallic nanoparticles within an arbitrary trapping range is a major challenge.

In this work, we propose a strategy for formation of a stable 3D optical trap for a resonant metallic nanoparticle using the 4π high numerical aperture (NA) focusing system by elongating a tightly focused field in the transverse direction. Unlike cylindrically symmetrical optical traps, we have demonstrated that 50-nm-diameter gold nanoparticles are trapped in a linear potential well when illuminated using shaped optical fields at a wavelength of 532 nm. We analyzed the trapping range and the trapping force of this linear trap along with the dependence of these effects on the incident light polarization. Through

* Corresponding author at: School of Physics and Optoelectronic Engineering, Shandong University of Technology, Zibo 255000, China.
E-mail address: zsman@sdut.edu.cn (Z. Man).

https://doi.org/10.1016/j.optcom.2020.126045
Received 29 February 2020; Received in revised form 24 April 2020; Accepted 29 April 2020
Available online 30 April 2020

a detailed force-field analysis, it is found that gold nanoparticles can be trapped within a long range of 5.468λ, where λ is the wavelength, and the corresponding maximum optical force and potential depth are calculated to be 0.547 pN and $51.4k_BT$ along the x-axis, respectively, where k_B is the Boltzmann constant. In addition, the trapping range can be adjusted easily by varying one of the parameters as desired. This technology provides a whole new optical tweezers configuration that will help to open up new avenues for optical trapping.

2. Theoretical approach

It is difficult to perform 3D confinement of metallic particles using a single focused laser beam because the strong axial scattering force pushes the metallic particles away from the focal spot. One potentially viable approach is to cancel the effect of the axial scattering force on the metallic particles using the symmetry of the 4π focusing system. To this end, we construct a 4π focusing system that consists of two high-NA objectives illuminated using two counterpropagating vector beams, as shown in Fig. 1. We consider here that the electric field distribution of the initial incident light with homogeneous linear polarization can be expressed as

$$\mathbf{E}_0 = A_0 \left(\cos c_0 \mathbf{e}_x + \sin c_0 \mathbf{e}_y\right), \tag{1}$$

where A_0 is the amplitude constant and c_0 is the initial electric field vector orientation with respect to the x axis. $\mathbf{e}_x$ and $\mathbf{e}_y$ are the unit vectors corresponding to the x and y directions, respectively.

The Pancharatnam–Berry (PB) phase is a geometric phase associated with the polarization of light that can manipulate the polarization to create vector beams [34–39]. To obtain the ideal highly-confined focal field distributions required in the focusing system, a special PB phase is designed to tailor the polarization state of the input field $\mathbf{E}_0$. The corresponding input field $\mathbf{E}_{in}$ is expressed as

$$\mathbf{E}_{in} = A_0 \left\{\cos\left[2\pi t\left(\frac{r\cos\varphi}{r_0}\right)^3 + c_0\right]\mathbf{e}_x + \sin\left[2\pi t\left(\frac{r\cos\varphi}{r_0}\right)^3 + c_0\right]\mathbf{e}_y\right\}, \tag{2}$$

where r and φ are the polar radius and the azimuthal angle in the polar coordinate system, respectively, and r_0 is the input field radius; t is the phase index, which in theory can have any integer value. For a nonzero value of t, the input beam has spatially varying states of polarization. The diagram of the optical tweezers in Fig. 1 below shows the polarization distributions of the two counter-propagating vector beams with phase indexes of $(t_L, t_R) = (16, -16)$. Here, t_L and t_R stand for the phase indexes of the left and right incident beams, respectively.

Richards and Wolf's vectorial diffraction theory [40] can be used to determine the electric fields in the vicinity of the focus of the counter-propagating incident beams in the 4π focusing system:

$$\mathbf{E}_L\left(\rho_p,\phi_p,z_p\right) = \begin{bmatrix} E_{L_x} \\ E_{L_y} \\ E_{L_z} \end{bmatrix} = \frac{-ikfl_0}{2\pi}\int_0^{2\pi}\int_0^{\theta_{\max}} \sqrt{\cos\theta}\, l(\theta)\sin\theta \begin{bmatrix} L_1 \\ L_2 \\ L_3 \end{bmatrix} \times e^{\left\{ik\left[-\rho_p\sin\theta\cos\left(\varphi-\phi_p\right)+z_p\cos\theta\right]\right\}}\mathrm{d}\theta\mathrm{d}\varphi, \tag{3}$$

$$\mathbf{E}_R\left(\rho_p,\phi_p,z_p\right) = \begin{bmatrix} E_{R_x} \\ E_{R_y} \\ E_{R_z} \end{bmatrix} = \frac{-ikfl_0}{2\pi}\int_0^{2\pi}\int_0^{\theta_{\max}} \sqrt{\cos\theta}\, l(\theta)\sin\theta \begin{bmatrix} R_1 \\ R_2 \\ R_3 \end{bmatrix} \times e^{\left\{ik\left[-\rho_p\sin\theta\cos\left(\varphi-\phi_p\right)-z_p\cos\theta\right]\right\}}\mathrm{d}\theta\mathrm{d}\varphi, \tag{4}$$

where $\mathbf{E}_L$ and $\mathbf{E}_R$ denote the focal electric fields of the left and right objectives, respectively. ρ_p, ϕ_p, and z_p are the cylindrical coordinates of an arbitrary point P within the focal region. l is an amplitude factor related to the power of the incident field, f is the focal length, and $k = 2\pi n_1/\lambda$ is the wave vector in the image space; λ is the wavelength of the incident wave; and $\theta_{\max} = \arcsin(\mathrm{NA}/n_1)$ is the maximum convergence angle, where n_1 denotes the refractive index in the image space. $l(\theta)$ represents the amplitude distribution of the incident beam in the pupil plane of the objective and is considered as [41]:

$$l(\theta) = \exp\left[-\beta^2\left(\frac{\sin\theta}{\sin\theta_{\max}}\right)^2\right] J_1\left(2\beta\frac{\sin\theta}{\sin\theta_{\max}}\right), \tag{5}$$

where β is the ratio of the pupil radius to the beam waist and J_1 is the first-order Bessel function of the first kind.

L_j (j = 1, 2, and 3) and R_j (j = 1, 2, and 3) represent the three orthogonal polarization components in the image space, which are determined by the input polarization states in the left and right sides, respectively. Using Eqs. (3) and (4), the relationships between L_j and R_j can be expressed as follows:

$$R_1 = L_1 = \sin\left[\varphi - 2\pi t\left(\frac{\sin\theta\cos\varphi}{\sin\theta_{\max}}\right)^3 - c_0\right]\sin\varphi + \cos\left[2\pi t\left(\frac{\sin\theta\cos\varphi}{\sin\theta_{\max}}\right)^3 + c_0 - \varphi\right]\cos\theta\cos\varphi, \tag{6}$$

$$R_2 = L_2 = \sin\left[2\pi t\left(\frac{\sin\theta\cos\varphi}{\sin\theta_{\max}}\right)^3 + c_0 - \varphi\right]\cos\varphi + \cos\left[2\pi t\left(\frac{\sin\theta\cos\varphi}{\sin\theta_{\max}}\right)^3 + c_0 - \varphi\right]\cos\theta\sin\varphi, \tag{7}$$

$$R_3 = -L_3 = -\sin\theta\cos\left[2\pi t\left(\frac{\sin\theta\cos\varphi}{\sin\theta_{\max}}\right)^3 + c_0 - \varphi\right]. \tag{8}$$

Therefore, the total electric field at an arbitrary point P in the focal region is given by the vector superposition of the electric fields from the left and right targets. This is expressed as

$$\mathbf{E}_{\text{total}}\left(\rho_p,\phi_p,z_p\right) = \mathbf{E}_L\left(\rho_p,\phi_p,z_p\right) + \mathbf{E}_R\left(\rho_p,\phi_p,z_p\right). \tag{9}$$

Eqs. (2)–(9) demonstrate that it is possible to control the shape of the objective electric field constructively by manipulating the polarization patterns of the incident beams, which are determined using the phase index t.

To illustrate the strength of the interaction between a nanostructure and such an optical field, we assume that a Rayleigh spherical particle with relative permittivity ε_2 is placed in the focused fields in a medium with a dielectric constant of ε_1 and its optical properties are then characterized as follows using the polarizability α [24]:

$$\alpha = \frac{\alpha_0}{1 - ik^3\alpha_0/6\pi\varepsilon_0} \quad \alpha_0 = 4\pi\varepsilon_0 a^3\frac{\varepsilon_2 - \varepsilon_1}{\varepsilon_2 + 2\varepsilon_1}, \tag{10}$$

where ε_0 is the vacuum permittivity and a is the radius of the nanoparticle. The time-averaged light-induced forces acting on the Rayleigh particle can be written as the sum of two terms: the gradient force and the scattering force. The gradient force is proportional to the gradient of the electric field intensity and its purpose is to confine the particles toward the center of the focus; this force can be written as

$$\mathbf{F}_{grad} = \frac{1}{4}\mathrm{Re}(\alpha)\nabla|\mathbf{E}|^2. \tag{11}$$

In free space, the scattering force acting on the Rayleigh particle is usually considered to be proportional to the Poynting vector when the light is linearly polarized. However, the curl force associated with the nonuniform spin density distribution of the light field makes an additional contribution to the scattering force in the nonuniform helical light field [24]. Therefore, we can finally write the total scattering force as:

$$\mathbf{F}_{scat} = \frac{\sigma}{2c}\mathrm{Re}\left(\mathbf{E}\times\mathbf{H}^*\right) + \sigma c\nabla\times\left[\frac{\varepsilon_0}{4\omega i}\left(\mathbf{E}\times\mathbf{E}^*\right)\right], \tag{12}$$

where $\varepsilon_0(\mathbf{E}\times\mathbf{E}^*)/(4\omega i)$ is the well-known time averaged spin density of a transverse electromagnetic field [42–44]. c is the speed of light, $\mathbf{H}$ is the magnetic field, $\sigma = k\,\mathrm{Im}(\alpha)/\varepsilon_0$ is the extinction cross-section, and w is the angular frequency of the electromagnetic field. The first term is the radiation pressure caused by the momentum transferred from the photons in the beam, the second term is the curl force that arises as a

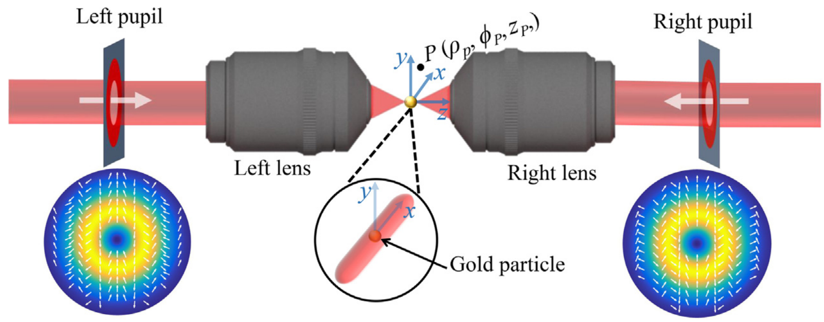

Fig. 1. Schematic of the optical tweezers using the 4π high-NA objective lens-focusing system.

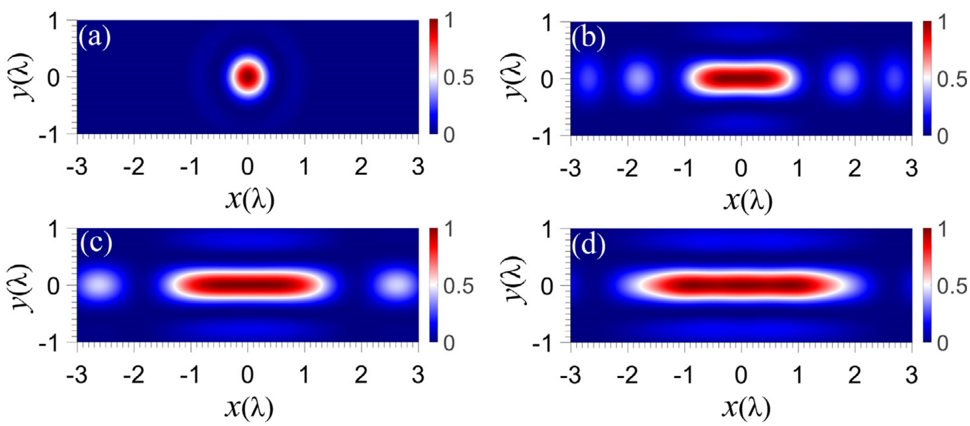

Fig. 2. Normalized intensity distributions of tightly focused input beams in the x–y plane with phase indexes (t_L, t_R) of (a) (0, 0), (b) (2, −2), (c) (6, −6), and (d) (16, −16).

reaction of the particle in opposition to the rotation of the spin, and the total scattering force is proportional to the total particle cross-section σ.

3. Results and discussion

After some numerical calculations, we found that when two counter-propagating beams are incident on the objective, an elliptically-shaped focal spot can be generated within the focal region when t_L and t_R are opposite to each other. For all the following calculations, $t_L = -t_R$ is chosen. We initially used four pairs of input fields with phase indexes (t_L, t_R) of (0, 0), (2, −2), (6, −6), and (16, −16) to investigate the intensity distribution of the focused electrical field. The objective lens NA = 0.95, the image space refractive index $n_1 = 1.333$, and the ratio $\beta = 1$. Fig. 2(a)–(d) show the corresponding normalized electric field intensity profiles in the focal plane for the input beams when focused using the 4π focusing system. Unlike Fig. 2(b)–(d), where the intensity shows a linear shape, the uniform polarization illumination with (t_L, t_R) = (0, 0) generates a sharp focal spot, as illustrated in Fig. 2(a). When the phase index has a nonzero value, the full width at half maximum (FWHM) values along the y-axis direction appear to be suppressed by the 4π system, and the FWHM in the y direction (W_y), the same quantity in the x direction (W_x), and the strengths of the side lobes are tunable using the phase index of the input field (Fig. 2(b)–(d)). It is found that a remarkable, almost needle-like (aspect ratio of 0.114) focal spot with subwavelength width can be realized at the focal region when (t_L, t_R) = (16, −16). The calculated values of W_x are 1.701λ and 2.592λ for (t_L, t_R) = (2, −2) and (6, −6), respectively, while the corresponding values of W_y are 0.440λ and 0.430λ, respectively, which are both smaller than the diffraction limit for the objective lenses given by $\lambda/(2\mathrm{NA}) = 0.526\lambda$. To provide further verification of these analyses, we plot the corresponding line-scans of the x axis intensity distributions (Fig. 3(a)) and the quantitative relationships between t_L and both W_x and W_y (Fig. 3(b)). It is obvious that the intensity uniformity becomes stronger when the focus is elongated (Fig. 3(a)), which leads to a descent in the intensity gradient. To evaluate the uniformity of the linear focal spot along the x-axis, a uniformity factor is defined as $Q = 2I_{min}/(I_{max} + I_{min})$ [45], where I_{max} and I_{min} represent the maximum and minimum intensities along the x-axis, respectively. The uniformity in the central 2λ area is approximately 96% when (t_L, t_R) = (16, −16). In addition, the results clearly show that as t_L increases, W_x decreases while W_y increases (Fig. 3(b)). As a result, we have achieved a linear focal spot with controllable length and a subwavelength width in the transverse plane, which acts as new optical tweezers for optical manipulation applications.

To illustrate the trapping properties of these novel optical tweezers, it is essential to understand the most challenging situation that they face. When the illumination wavelength approaches the wavelength that corresponds to the peak of the absorption cross-section (ACS) (which is also known as the absorption resonance), the two main challenges for trapping of metallic nanoparticles are as follows: (i) the scattering force is maximized because the absorption peak wavelength corresponds to the maximum of the imaginary part of the polarizability; and (ii) the thermal effect is more significant at the peak of the ACS because the ACS is used to measure the strength of the nanoparticle's absorption of the photons. Therefore, we present here the most challenging situation to be faced when attempting to achieve 3D trapping of a metallic nanoparticle in the absorption resonance band. Consider a gold nanoparticle with a radius of 50 nm immersed in water (n_1 = 1.333, ε_1 = 1.77). The index of refractive of the gold nanoparticle is 0.467 + 2.4083i [27] when the illumination wavelength is 532 nm (wavelength corresponding to the peak of the ACS). The incident power is assumed to be 100 mW. Using Eqs. (1)–(12), we investigated both the distributions and the magnitudes of the resulting optical forces that are exerted on the gold nanoparticle.

Fig. 4 illustrates the transverse optical force distributions on the gold nanoparticle produced by focusing of different input fields along

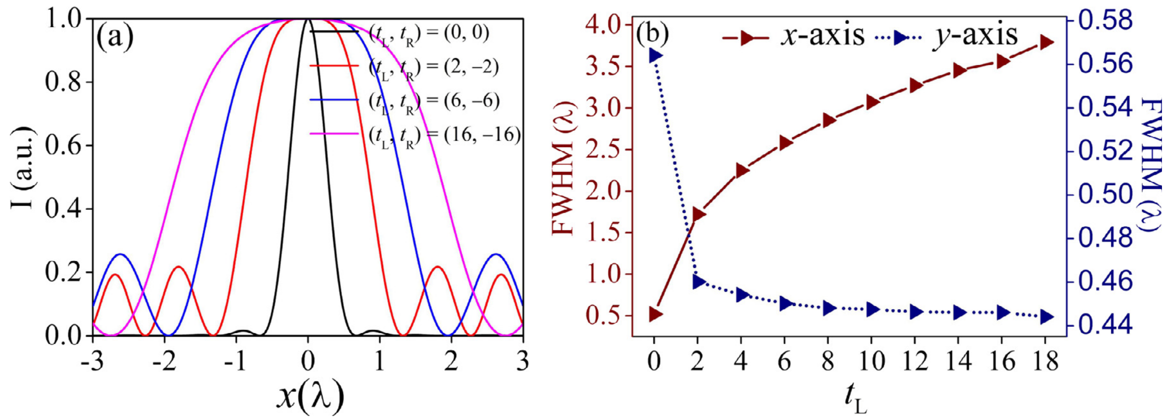

Fig. 3. (a) Line scans of intensity distributions along the x axis. (b) FWHM values of the tightly focused fields along the x and y directions with NA = 0.95 versus t_L. For all the calculations, $t_L = -t_R$ is chosen.

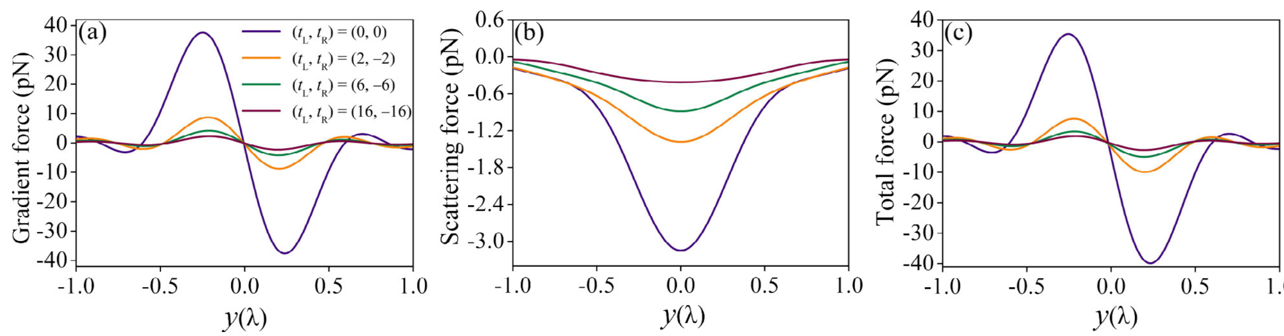

Fig. 4. Transverse optical force distributions of the gold nanoparticle along the y-axis produced using tightly focused optical fields with phase indexes (t_L, t_R) of (0, 0), (2, −2), (6, −6), and (16, −16). (a) Transverse gradient force along the y-axis. (b) Transverse scattering force along the y-axis. (c) Summation of the transverse gradient and scattering forces acting along the y-axis.

the y-axis. The total optical force here is given by the vector superposition of the gradient and scattering forces and the total optical force is defined as $\mathbf{F}_{grad} + \mathbf{F}_{scat}$. It is shown that the gradient forces near the geometric focus all demonstrate restoring force behavior (Fig. 4(a)), and the maximal gradient force of the cylindrically symmetrical optical trap is greater than that of the linear optical trap. Unlike the gradient force, the scattering force distribution is sunken, with the focus at the center and a negative magnitude along the y-axis (Fig. 4(b)). Furthermore, the gradient force dominates the total optical force distribution in all cases (Fig. 4(c)) and the gold nanoparticle can be trapped near the focus along the y-axis because the total optical forces acting on either side of the focus provide an opposing effect on the particle.

Similarly, Fig. 5 shows the transverse optical forces exerted on the gold particle along the x-axis. For a cylindrically symmetrical optical trap, the gradient force magnitude acting along the x-axis is comparable with that acting along the y-axis. With the linear optical trap, the maximal x-axis gradient force F_x^{gmax} is obviously smaller than the corresponding y-axis force F_y^{gmax}. This is because, for a Rayleigh particle, the gradient force is proportional to the intensity gradient of the focused beam. For a linear optical trap, the intensity gradient along the y-axis appears to be greater than that along the x-axis. Notably, the magnitude of the scattering forces is negligible when compared with that of the gradient forces. Therefore, the distribution trends for the total optical force and the gradient force are basically the same. In addition, the total force is always directed toward the focal point position to produce a force balance.

The trapping range is an important index for evaluation of the trapping ability of an optical trap. The trapping range of the optical trap, denoted by R, is defined as twice the continuous length of the positive total force acting on the left side of an equilibrium point. By analyzing the total optical force distributions, the transverse trapping range of the optical trap can be determined and $R/2$ is also shown in Fig. 5(c1)–(c4). These results show that while the cylindrically symmetrical optical trap is able to generate the maximal trapping force, its trapping range is relatively short (1.177λ) (Fig. 5(c1)). The trapping range for a linear optical trap can be tuned by adjusting the phase index of the incident field. The maximum trapping range of the linear optical trap is approximately five times larger than that of the cylindrically symmetrical optical trap (Fig. 5(c1) and (c4)). Generally, there is a trade-off between the trapping force and the trapping range. Because the magnitude of the trapping force is correlated with the incident laser power, the trapping force can be modulated by varying the power of the incident beam when a larger trapping range is obtained. The condition for stable optical trapping is that the potential depth of the optical trap must be sufficient to overcome the kinetic energy of the particles in Brownian motion, $k_B T$, where k_B is the Boltzmann constant and T is the temperature of the environment surrounding the particle, which is assumed to be 293 K. The trapping potential of the linear optical trap is estimated using $U = -\int \mathrm{F} \cdot \mathbf{ds}$ [27], which represents the work done by the optical force along the trapping length direction. The computational results show that the minimum potential depths along the x and y directions are $51k_B T$ and $62k_B T$, respectively, thus demonstrating that stable trapping can be realized in the transverse plane.

To create stable 3D trapping of the gold nanoparticle, we perform both numerical calculations and an analytical study of the axial optical force acting along the z direction (Fig. 6). The distributions of the optical forces in the case of a 2π focusing system illuminated by the incident beams are shown in Fig. 6(a1)–(c1). Unlike the transverse forces in the focal plane, which mainly originate from the gradient forces (Figs. 4 and 5), the axial scattering force is greater than the gradient force (Fig. 6(a1) and (b1)). The results show that the positive axial scattering force is generated in the focal region, where it becomes

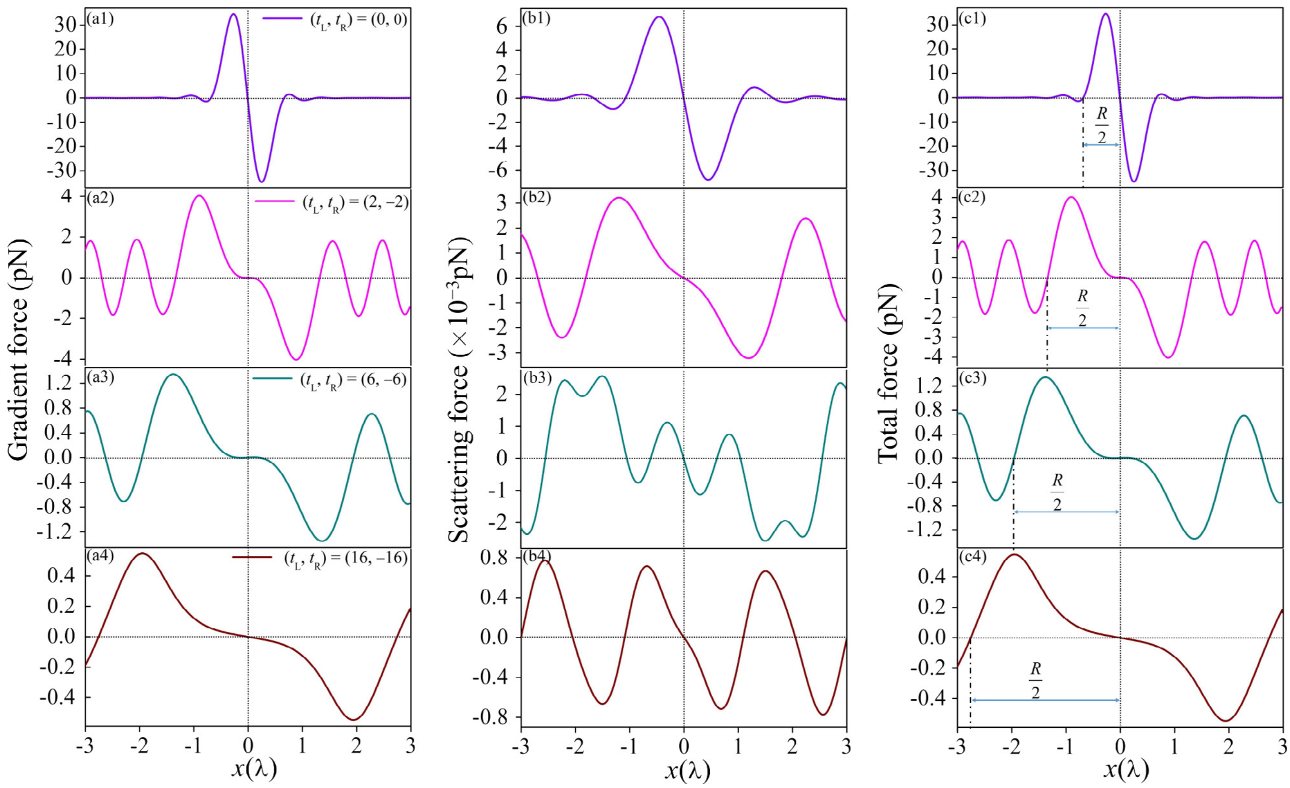

Fig. 5. Transverse optical force distributions for the gold nanoparticle along the x-axis produced using tightly focused optical fields with phase indexes (t_L, t_R) of (0, 0), (2, −2), (6, −6), and (16, −16). (a1)–(a4) Transverse gradient forces along the x-axis. (b1)–(b4) Transverse scattering forces along the x-axis. (c1)–(c4) Summation of these transverse gradient and scattering forces along the x-axis.

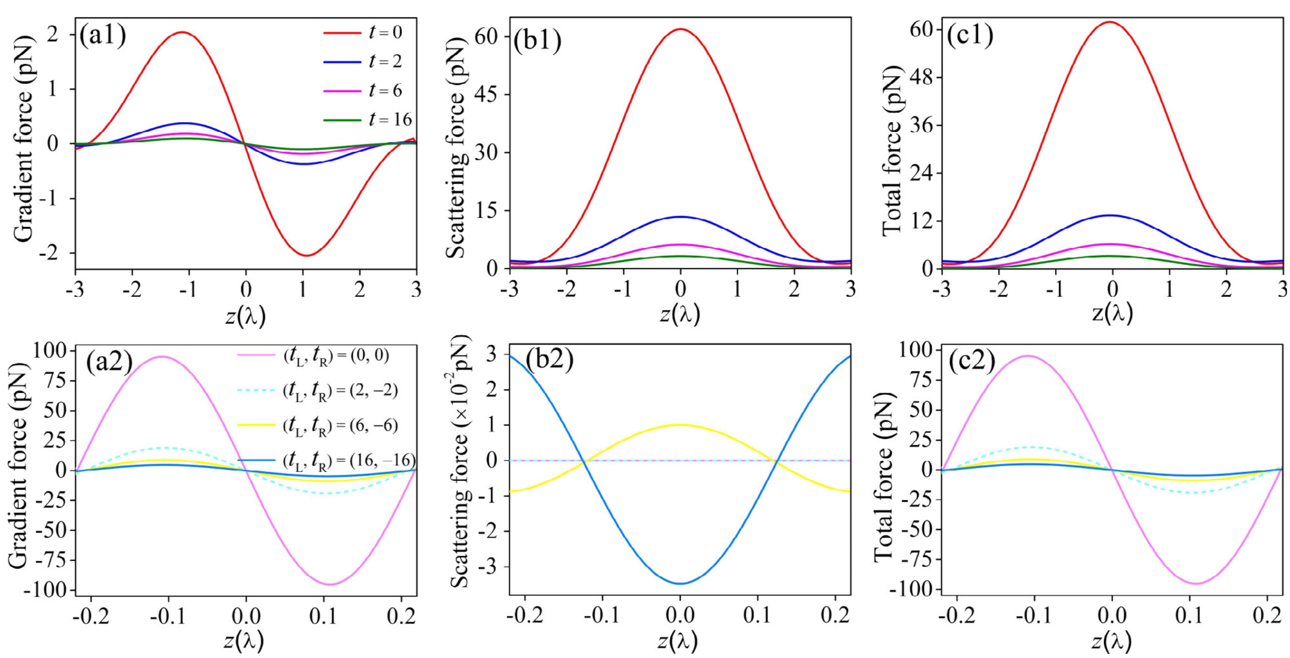

Fig. 6. Axial optical force distributions along the z direction for the gold nanoparticle produced in (a1)–(c1) the 2π focusing system and (a2)–(c2) the 4π focusing system using tightly focused optical fields with phase indexes (t_L, t_R) of (0, 0), (2, −2), (6, −6), and (16, −16).

dominant over the total optical force. The gold nanoparticle will be pushed axially away from the focus because of the strong positive longitudinal optical force. Consequently, the capability for 3D trapping of particles using the 2π focusing system is then disabled. When compared with the 2π focusing system case, this axial scattering force is reduced because of the symmetry of the 4π focusing system. The results show that the axial gradient force has been enhanced in the 4π focusing system and dominates the total optical force distributions. Obviously, an equilibrium point at $z = 0$ still exists along the optical axis (Fig. 6(c1)), and the minimum potential depth is calculated to be $80k_BT$. As a result, 3D trapping of the gold nanoparticle is realized under the resonance condition.

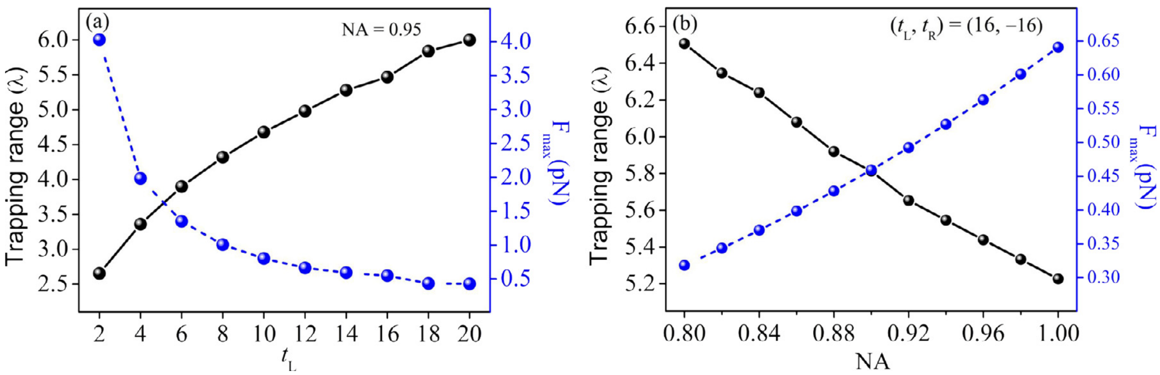

Fig. 7. Changes in trapping range and maximum optical force F_{max} along the x direction with (a) phase index t_L and (b) the NA of the objective lens. For all the calculations in this figure, $t_L = -t_R$ is chosen.

In addition to the phase index t, the maximum optical force F_{max} exerted on the gold nanoparticle and the trapping range of the optical trap are strongly dependent on the NA of the objective lens. The dependences of the trapping range and F_{max} along the x direction on t and the NA are investigated quantificationally as shown in Fig. 7. In Fig. 7(a), we set the NA to be 0.95 and vary t_L, whereas in Fig. 7(b), the phase indexes are set at $(t_L, t_R) = (16, -16)$, and the NA is varied. We find that an increase in t_L results in a reduction in F_{max} and an increase in the trapping range, which agrees well with the results of the previous analysis shown in Fig. 5. In contrast to the results shown in Fig. 7(a), the value of F_{max} increases with increasing NA, and the trapping range also decreases with an increase in the NA (as shown in Fig. 7(b). In particular, the optical trap has a stronger trapping capability and greater trap stiffness when a higher trapping force is exerted on the particles. However, the results show that the trapping range variation trend is always opposite to that of F_{max}. Therefore, to increase both the trapping range and the trap stiffness in the optical tweezers simultaneously, we must balance t_L with the NA.

4. Conclusions

In conclusion, we have proposed a novel optical tweezers configuration to enable 3D trapping of a metallic nanoparticle. By focusing two counterpropagating vector beams using two high-NA aplanatic objective lenses, a transverse enhanced optical field can be created within the focal plane by tailoring the polarizations of the incident fields. We have studied the characteristics of the transverse and longitudinal optical forces for a gold nanoparticle. The analysis results show that the gold nanoparticle can be trapped stably in the proposed optical trap. Additionally, the transverse trapping range can be adjusted via the simultaneous and independent control of the phase index t and the NA and the range increases with increasing t_L or decreasing NA. It should be noted that the trapping range should be enlarged while keeping the magnitudes of the optical forces in mind, because the optical forces that are exerted on the nanoparticles are directly related to both the trapping efficiency and the stiffness. This novel trapping method will hopefully be applicable to other types of nanoparticles, e.g., ellipsoidal-shaped metallic nanoparticles, semiconductor nanowires and carbon nanotubes, thus opening up new paths for optical manipulation of these materials. It should also be emphasized that the incident two beams need to be precisely aligned in practical applications.

Declaration of competing interest

The authors declare that they have no known competing financial interests or personal relationships that could have appeared to influence the work reported in this paper.

Acknowledgments

National Natural Science Foundation of China (NSFC) (11604182, 11704226); Natural Science Foundation of Shandong Province, China (ZR2016AB05); Natural Science Foundation of Shandong Province, China (ZR2017MA051).

References

[1] A. Ashkin, Acceleration and trapping of particles by radiation pressure, Phys. Rev. Lett. 24 (1970) 156–159.
[2] A. Ashkin, Trapping of atoms by resonance radiation pressure, Phys. Rev. Lett. 40 (1978) 729–732.
[3] A. Ashkin, J.M. Dziedzic, J.E. Bjorkholm, S. Chu, Observation of a single-beam gradient force optical trap for dielectric particles, Opt. Lett. 11 (1986) 288–290.
[4] Y.F. Chen, X. Serey, R. Sarkar, P. Chen, D. Erickson, Controlled photonic manipulation of proteins and other nanomaterials, Nano Lett. 12 (2012) 1633–1637.
[5] R. Agarwal, K. Ladavac, Y. Roichman, G.H. Yu, C.M. Lieber, D.G. Grier, Manipulation and assembly of nanowires with holographic optical traps, Opt. Express 13 (2005) 8906–8912.
[6] G. Rui, Q.W. Zhan, Tailoring optical complex fields with nano-metallic surfaces, Nanophotonics 4 (2015) 2–25.
[7] M. Meier, V. Romano, T. Feurer, Material processing with pulsed radially and azimuthally polarized laser radiation, Appl. Phys. A Mater. Sci. Process. 86 (2007) 329–334.
[8] M. Beresna, M. Gecevičius, P.G. Kazansky, T. Gertus, Radially polarized optical vortex converter created by femtosecond laser nanostructuring of glass, Appl. Phys. Lett. 98 (2011) 201101.
[9] S.N. Olof, J.A. Grieve, D.B. Phillips, H. Rosenkranz, M.L. Yallop, M.J. Miles, D.M. Carberry, Measuring nanoscale forces with living probes, Nano Lett. 12 (2012) 6018–6023.
[10] D.B. Phillips, G.M. Gibson, R. Bowman, M.J. Padgett, S. Hanna, D.M. Carberry, S.H. Simpson, An optically actuated surface scanning probe, Opt. Express 20 (2012) 29679–29693.
[11] K. Dholakia, P. Zemánek, Colloquium: gripped by light: optical binding, Rev. Modern Phys. 82 (2010) 1767–179.
[12] P.C. Chaumet, M. Nieto-Vesperinas, Optical binding of particles with or without the presence of a flat dielectric surface, Phys. Rev. B 64 (2001) 035422.
[13] E. Almaas, I. Brevik, Possible sorting mechanism for microparticles in an evanescent field, Phys. Rev. A 87 (2013) 063826.
[14] M.M. Wang, E. Tu, D.E. Raymond, J.M. Yang, H. Zhang, N. Hagen, P.J. Marchand, Microfluidic sorting of mammalian cells by optical force switching, Nat. Biotechnol. 23 (2005) 83–87.
[15] J.R. Moffitt, Y.R. Chemla, S.B. Smith, C. Bustamante, Recent advances in optical tweezers, Annu. Rev. Biochem. 77 (2008) 205–228.
[16] I. Heller, T.P. Hoekstra, G.A. King, E.J.G. Peterman, G.J.L. Wuite, Optical tweezers analysis of DNA-protein complexes, Chem. Rev. 114 (2014) 3087–3119.
[17] L. Huang, H. Guo, J. Li, L. Ling, B. Feng, Z.Y. Li, Optical trapping of gold nanoparticles by cylindrical vector beam, Opt. Lett. 37 (2012) 1694–1696.
[18] P. Shi, L.P. Du, X.C. Yuan, Structured spin angular momentum in highly focused cylindrical vector vortex beams for optical manipulation, Opt. Express 26 (2018) 23449–23459.
[19] E. Vetsch, D. Reitz, G. Sague, R. Schmidt, S.T. Dawkins, A. Rauschenbeutel, Optical interface created by laser-cooled atoms trapped in the evanescent field surrounding an optical nanofiber, Phys. Rev. Lett. 104 (2010) 203603–203604.

[20] C.J. Min, A. Shen, J.F. Shen, Y.Q. Zhang, H. Fang, G.H. Yuan, L.P. Du, S.W. Zhu, T. Lei, X.C. Yuan, Focused plasmonic trapping of metallic particles, Nature Commun. 4 (2013) 2891.

[21] A. Canaguier-Durand, A. Cuche, C. Genet, T.W. Ebbesen, Force and torque on an electric dipole by spinning light fields, Phys. Rev. A 88 (2013) 033831.

[22] G.H. Rui, Y. Li, S.C. Zhou, Y.S. Wang, B. Gu, Y.P. Cui, Q.W. Zhan, Optically induced rotation of Rayleigh particles by arbitrary photonic spin, Photonics Res. 7 (2019) 69–79.

[23] P.M. Hansen, V.K. Bhatia, N. Harrit, L. Oddershede, Expanding the optical trapping range of gold, Nano Lett. 5 (2015) 1937–1942.

[24] S. Albaladejo, M.I. Marqués, M.V. Laroche, J.J. SáenzV, Scattering forces from the curl of the spin angular momentum of a light field, Phys. Rev. Lett. 102 (2009) 113602.

[25] Y.J. Zhang, B.F. Ding, T.K. Suyama, Trapping two types of particles using a double-ring-shaped radially polarized beam, Phys. Rev. A 81 (2010) 023831.

[26] K. Ding, J. Ng, L. Zhou, C.T. Chan, Realization of optical pulling forces using chirality, Phys. Rev. A 89 (2014) 063825.

[27] G.H. Rui, Q.W. Zhan, Trapping of resonant metallic nanoparticles with engineered vectorial optical field, Nanophotonics 3 (2014) 351–361.

[28] X. Y.Wang, G.H. Rui, L.P. Gong, B. Gu, Y.P. Cui, Manipulation of resonant metallic nanoparticle using 4pi focusing system, Opt. Express 24 (2016) 24143–24152.

[29] Y.Q. Zhang, J.F. Shen, C.J. Min, Y.F. Jin, Y.Q. Jiang, J. Liu, S.W. Zhu, Y.L. Sheng, V.Z. Anatoly, X.C. Yuan, Nonlinearity-induced multiplexed optical trapping and manipulation with femtosecond vector beams, Nano Lett. 18 (2018) 5538–5543.

[30] Y.Q. Zhang, X.J. Dou, Y.M. Dai, X.Y. Wang, C.J. Min, X.C. Yuan, All-optical manipulation of micrometer-sized metallic particles, Photon. Res. 6 (2018) 66–71.

[31] Y.H. Bai, M. Dong, M.Y. Zhang, Y.J. Yang, Properties of a tightly focused circularly polarized anomalous vortex beam and its optical forces on trapped nanoparticles, Nanoscale Res. Lett. 14 (2019) 252.

[32] Y.B. Ma, G.H. Rui, B. Gu, Y.P. Cui, Trapping and manipulation of nanoparticles using multifocal optical vortex metalens, Sci. Reps. 7 (2017) 14611.

[33] X. Li, H. Ma, H. Zhang, M. Tang, H. Li, J. Tang, Y. Wang, Is it possible to enlarge the trapping range of optical tweezers via a single beam?, Appl. Phys. Lett. 114 (2019) 081903.

[34] Z. Bomzon, V. Kleiner, E. Hasman, Pancharatnam-berry phase in space-variant polarization-state manipulations with subwavelength gratings, Opt. Lett. 26 (2001) 1424–1426.

[35] J.B. Mueller, N.A. Rubin, R.C. Devlin, B. Groever, F. Capasso, Metasurface polarization optics: Independent phase control of arbitrary orthogonal states of polarization, Phys. Rev. Lett. 118 (2017) 113901.

[36] Z. Man, P.W. Meng, S.G. Fu, Creation of complex nano-interferometric field structures, Opt. Lett. 45 (2020) 37–40.

[37] T.C. Liu, Y.G. Ke, J.K. Zhou, Y.Y. Liu, H.L. Luo, S.C. Wen, D.Y. Fan, Generation of perfect vortex and vector beams based on pancharatnam-berry phase elements, Sci. Rep. 7 (2017) 44096.

[38] Z. Man, X.J. Dou, S.G. Fu, Pancharatnam-berry phase shaping for control of the transverse enhancement of focusing, Opt. Lett. 44 (2019) 427–430.

[39] Z. Man, Z. Xi, X.C. Yuan, R.E. Burge, H. Paul Urbach, Dual coaxial longitudinal polarization vortex structures, Phys. Rev. Lett. 124 (2020) 103901–103906.

[40] B. Richards, E. Wolf, Electromagnetic diffraction in optical systems. II. Structure of the image field in an aplanatic system, Proc. R. Soc. Lond. Ser. A Math. Phys. Eng. Sci. 253 (1959) 358–379.

[41] K.S. Youngworth, T.G. Brown, Focusing of high numerical aperture cylindrical-vector beams, Opt. Express 7 (2000) 77–87.

[42] A. Aiello, P. Banzer, M. Neugebauer, G. Leuchs, From transverse angular momentum to photonic wheels, Nat. Photonics 9 (2015) 789.

[43] S.S. Zhang, S.G. Fu, H.N. Zhang, X.L. Ge, Z.D. Bai, Y.D. Lyu, R. Zhao, Z.S. Man, Fully controlled photonic spin in highly confined optical field, Opt. Express 27 (2019) 33621–33633.

[44] P.W. Meng, Z. Man, A.P. Konijnenberg, H.P. Urbach, Angular momentum properties of hybrid cylindrical vector vortex beams in tightly focused optical systems, Opt. Express 27 (2019) 35336–35348.

[45] L.W. Zhu, M.Y. Sun, D.W. Zhang, J.J. Yu, J. Wen, J.N. Chen, Multifocal array with controllable polarization in each focal spot, Opt. Express 23 (2015) 24688–24698.